Cytokine 114 (2019) 47–60

Contents lists available at ScienceDirect

Cytokine

journal homepage: www.elsevier.com/locate/cytokine

Alveolar bone healing in mice genetically selected in the maximum (AIRmax) or minimum (AIRmin) inflammatory reaction

Priscila Maria Colavite[a], Andreia Espindola Vieira[b], Carlos Eduardo Palanch Repeke[c], Rafaella Pavanelli de Araujo Linhari[a], Raíssa Gonçalves Carneiro Spera De Andrade[a], Andrea Borrego[d], Marcelo De Franco[e], Ana Paula Favaro Trombone[f], Gustavo Pompermaier Garlet[a,*]

[a] Department of Biological Sciences, Bauru School of Dentistry, University of São Paulo, Bauru, SP, Brazil
[b] Histology and Embryology Laboratory, Institute of Biological and Health Sciences (ICBS), Federal University of Alagoas (UFAL), Maceió, AL, Brazil
[c] Department of Dentistry, Federal University of Sergipe, Lagarto, Sergipe, Brazil
[d] Laboratory of Immunogenetics, Butantan Institute, Secretary of Health, Government of the State of São Paulo, SP, Brazil
[e] Diagnostic Section, Pasteur Institute, Secretary of Health, Government of the State of São Paulo, SP, Brazil
[f] Department of Health Science, Universidade do Sagrado Coração, Bauru, SP, Brazil

ARTICLE INFO

Keywords:
Bone
Inflammation
Cytokine

ABSTRACT

The exact role of inflammatory immune response in bone healing process is still unclear, but the success of the alveolar bone healing process seems to be associated with a moderate and transitory inflammatory response, while insufficient or exacerbated responses seems to have a detrimental influence in the healing outcome. In this context, we performed a comparative analysis of mice strains genetically selected for maximum (AIRmax) or minimum (AIRmin) acute inflammatory response to address the influence of inflammation genes in alveolar bone healing outcome. Experimental groups comprised 8-week-old male or female AIRmax and AIRmin submitted to extraction of upper right incisor, and evaluated at 0, 3, 7, 14 and 21 days after upper incision extraction by micro-computed tomography (μCT), histomorphometry, birefringence, immunohistochemistry and molecular (PCRArray) analysis. Overall, the results demonstrate a similar successful bone healing outcome at the endpoint was evidenced in both AIRmin and AIRmax strains. The histormophometric analysis reveal a slight but significant decrease in blood clot and inflammatory cells density, as well a delay in the bone formation in AIRmax strain in the early times, associated with a decreased expression of BMP2, BMP4, BMP7, TGFb1, RUNX2, and ALP. The evaluation of inflammatory cells nature reveals increased GR1 + cells counts in AIRmax strain at 3d, associated with increased levels of neutrophil chemoattractants such as CXCL1 and CXCL2, and its receptor CXCR1, while F4/80 + cell prevails in AIRmin strain at 7d. Also, our results demonstrate a relative predominance of M2 macrophages in AIRmin strain, associated with an increased expression of ARG1, IL10, TGFb, while M1 macrophages prevail in AIRmax, which parallel with increased IL-1B, IL-6 and TNF expression. At late repair stage, AIRmax presents evidences of increased bone remodeling, characterized by increased density of blood vessels and osteoclasts in parallel with decreased bone matrix density, as well increased levels of MMPs, osteoclastogenic and osteocyte markers. In the view of contrasting inflammatory and healing phenotypes of AIRmin and AIRmax strains in other models, the unpredicted phenotype observed suggests the existence of specific QTLs (*Quantitative trait loci*) responsible for the regulation 'sterile' inflammation and bone healing events. Despite the similar endpoint healing, AIRmax strain delayed repair was associated with increased presence of neutrophils and M1 macrophages, supporting the association of M2 cells with faster bone healing. Further studies are required to clarify the elements responsible for the regulation of inflammatory events at bone healing sites, as well the determinants of bone healing outcome.

* Corresponding author at: Bauru School of Dentistry (FOB/USP), Department of Biological Sciences, Al. Octávio Pinheiro Brisola, 9-75, CEP 17012-901 Bauru, SP, Brazil.
E-mail address: garletgp@usp.br (G.P. Garlet).

https://doi.org/10.1016/j.cyto.2018.11.027
Received 4 October 2018; Received in revised form 9 November 2018; Accepted 27 November 2018
Available online 22 December 2018

1. Introduction

Bone is a complex and dynamic mineralized connective tissue characterized by constant remodeling, which involves coupled cycles of bone resorption and subsequent bone formation. Bone tissue also presents a considerable potential for healing, being the cooperative action of bone forming and resorptive cells essential to restore the architecture and function of damaged tissue [1–3].

The bone healing process involves an injury-triggered local inflammatory immune reaction, whose extent and intensity are thought to influence the healing process outcome [4–6]. Chronic and exacerbated inflammatory responses are usually associated with impaired healing [7–9]. Conversely, a transitory and moderate inflammatory process is thought to contributes to healing by promoting the local production of growth factors and mediating the chemotaxis of cells associated with the repair process [7–9]. Indeed, along the alveolar bone healing in C57Bl/6 mice, diverse inflammatory mediators are detected along the different stages of healing, reinforcing the potential involvement of host response in this process [10,11]. In this scenario, the 'constructive inflammation' concept is supported by the association between anti-inflammatory drugs and delayed bone healing [11,12] .

However, the majority of information linking inflammation with bone originates from chronic inflammatory osteolytic conditions, and the exact influence of inflammatory response nature and extent in bone healing outcome remains unclear [12–14]. In this setting, knockout mice strains have been a useful tool to demonstrate a cause-and-effect relationship between different pro- and anti-inflammatory cytokines and bone *in vivo* [15,16]. However, knockout (KO) mice, albeit of being a remarkable experimental tool, represent an extreme and non-natural situation where a given cell or mediator is completely absent. Consequently, unnatural KO-conditions do not mimic physiological individual variations that could account for the healing dissimilarities and deviations, such as the ones characteristically observed in humans [17]. Alternatively, the comparative analysis of mice strains with distinct inflammatory phenotypes could allow a cause-and-effect analysis of the inflammatory balance and bone healing outcome.

In this context, mice strains genetically selected for maximum (AIRmax) or minimum (AIRmin) acute inflammatory reaction, which also differ in chronic inflammatory responsiveness, comprise a useful model for studying the mechanisms linking inflammation to multiple outcomes [18,19]. Genetic studies indicated that the contrasting inflammatory responsiveness of AIRmin and AIRmax strains involves at least 11 QTLs (*Quantitative trait loci*) [20]. Additionally, subsequent studies identified six inflammatory QTLs associated with the tissue regeneration phenotype in AIR strains [21]. These loci, located on chromosomes 1, 7, 8, 12, 14, and 16, harbor several candidate genes for the characteristic AIR phenotypes [22]. Interestingly, in addition to the distinct inflammatory phenotypes AIRmin and AIRmax were also describe to present distinct healing capacities. Indeed, a study focused in ear soft tissue healing demonstrated that the AIRmax strain presents a high regenerative capacity when compared to AIRmin [23]. Importantly, favorable wound healing outcome was associated with leukocyte infiltration [23], reinforcing the potential link between inflammation and healing. Additionally, QTLs on chromosomes 1 and 14 were identified to modulate ear wound healing [23], with also points to possible common determinants of inflammatory and healing capacities in AIRmin and AIRmax strains.

In this context, we hypothesize that AIRmin and AIRmax strains, due to their distinct inflammatory responsiveness and healing potential, can also present distinct bone healing outcomes. Therefore, their comparative analysis can provide important information regarding the link between inflammation and bone healing. In this study, AIRmax and AIRmin mice were submitted to the extraction of the upper right incisor and comparatively evaluated regarding the intensity and nature of the inflammatory response along alveolar bone healing, as well as regarding the healing outcome evaluated by means of microtomographic, histological, histomorphometric and molecular analyses.

2. Materials and methods

2.1. Animals

Experimental groups comprised 8-week-old AIRmin and AIRmax mice (strains generated and bred at Butantan Institute, Sao Paulo, Brazil), maintained during the experimental period in the animal facility of FOB/USP. AIRmin and AIRmax strains were obtained through bidirectional genetic selection, starting with a genetically heterogeneous founder population (F0) produced by intercrossing eight isogenic strains of mice of independent origins (A/J, DBA/2J, P/J, SWR/J, SJL/J, CBA/J, BALB/cJ, and C57BL/6J) [18,23].The derived populations inflammatory phenotype was determined by the local exudation and leukocyte influx quantification in response to polyacrylamide beads (Biogel), which allowed the subsequent bidirectional intercrossing and the progressive divergence of the AIRmax and AIRmin lines in the inflammatory readouts, derived from homozygotic accumulation of alleles in QTL endowed with opposite and additive effects on the inflammatory response [18,23].Throughout the period of the study, mice were fed with sterile standard solid mice chow (Nuvital, Curitiba, PR, Brazil) and sterile water. Each experimental protocol was carried out using equivalent numbers of male and female mice. The experimental protocol was approved by the local Institutional Committee for Animal Care and Use following the Guide for the Care and Use of Laboratory Animals principles (CEEPA-FOB/USP, process # 003/2014).

2.2. Experimental protocol and mice tooth extraction model

Animals were submitted to extraction of upper right incisor as previously described [24]. Male or female AIRmax and AIRmin mice (N = 5/time/group) were anesthetized by intramuscular administration of 80 mg/kg of ketamine chloride (Dopalen, Agribrans Brasil LTDA) and 160 mg/kg of xylazine chloride (Anasedan, Agribrands Brasil LTDA) in the proportion 1:1, according to the animal body mass. Importantly, animals presenting fractured teeth during the extraction were excluded from further analysis. At the end of the experimental periods (0, 3, 7, 14 and 21 days post tooth extraction), the animals were killed with an excessive dose of anesthetic and the maxillae samples were collected. The maxillae samples were analyzed by micro-computed tomography (μCT), after the maxillae samples were dissected and prepared for histomorphometry and collagen birefringence analyses or molecular analyses.

2.3. Micro-computed tomography (μCT) assessment

The maxillae samples were scanned by the Skyscan 1174 System (Skyscan, Kontich, Belgium), at 50 kV, 800μA, with a 0.5 mm aluminium filter and 15% beam hardening correction, ring artifacts, reduction, 180 degrees of rotation and exposure range of 1 degree. Images were captured with 1304x1024 pixels and a resolution of 14 μm pixel size. Projection images were reconstructed using the NRecon software and three-dimensional images obtained by the CT-Vox software. Morphological parameters of trabecular bone microarchitecture were assessed using the CTAn software in accordance with the recommended guidelines [25]. A cylindrical region of interest (ROI) with an axis length of 3 mm (100 slices) and diameter of 1 mm was determined by segmenting the trabecular bone located from the coronal to apical thirds. Trabecular measurements included the tissue volume (TV, mm^3), bone volume (BV, mm^3) bone volume fraction (BV/TV, %), trabecular thickness (Tb.Th, mm), trabecular number (Tb.N, 1/mm), and trabecular separation (Tb.Sp, mm) [25,26].

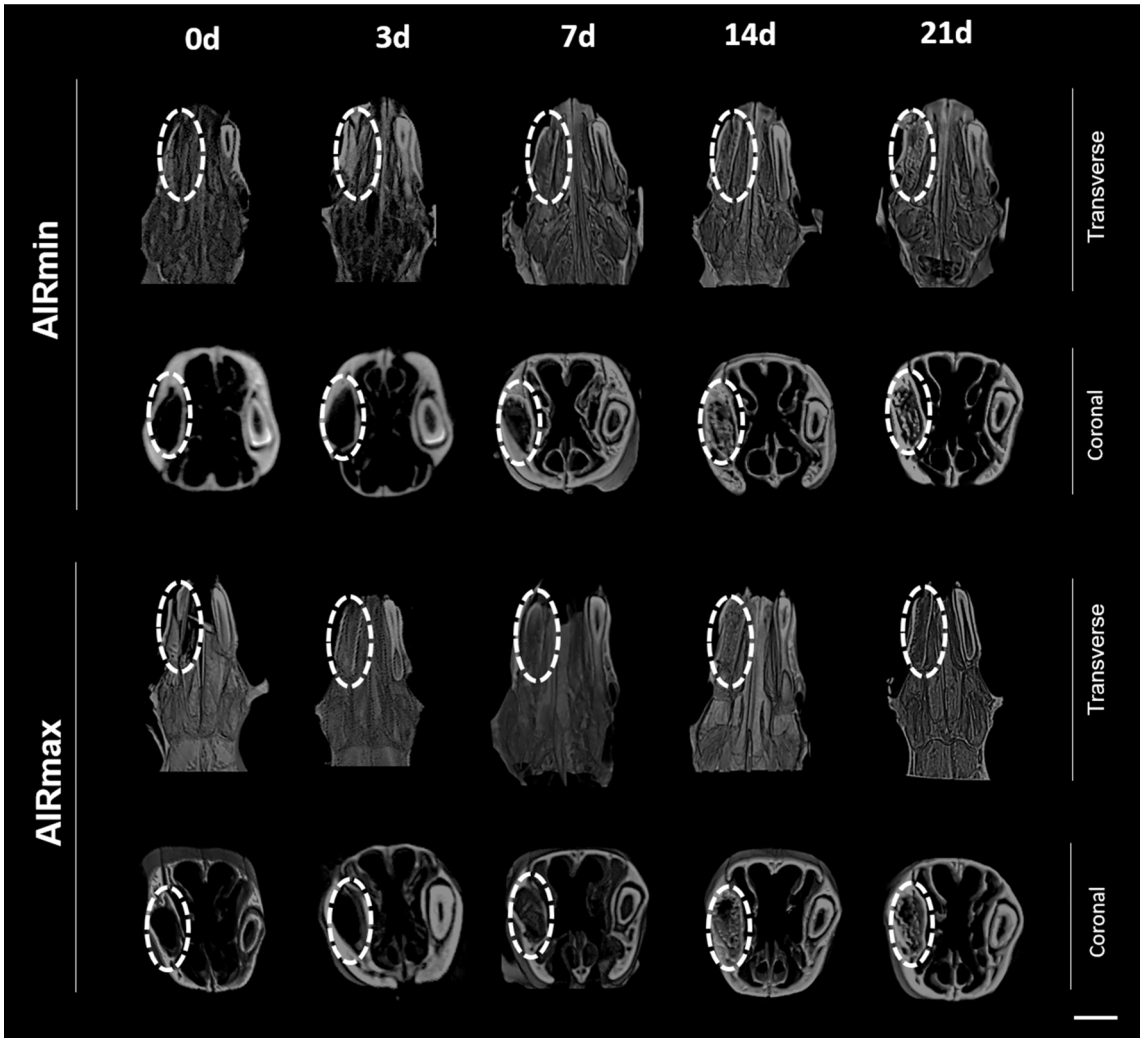

Fig. 1. Micro-computed tomography (μCT) analysis of bone healing process kinetics in AIRmin and AIRmax mice. Samples from 8-week-old male or female mice were scanned with the μCT System (Skyscan 1174; Skyscan, Kontich, Belgium) 0, 3, 7, 14 and 21 days post tooth extraction time points for the kinetics evaluation of the bone healing process. Images were reconstructed using the NRecon software and three-dimensional images obtained with the CT-Vox software. The sectioned maxilla are represented at the transverse and coronal planes. The delimited area is representing the bone healing process kinetics in mice.

2.4. Histomorphometric analysis

Serial sections (8 semi-serial sections of each maxilla, with a 5 μm thickness for each section) were obtained using a microtome (Leica RM2255, Germany) and stained with H.E. (hematoxylin and eosin). Morphometric measurements were performed by a single calibrated investigator with a binocular light microscope (Olympus Optical Co., Tokyo, Japan) using a 100x immersion objective and a Zeiss kpl 8X eyepiece containing a Zeiss II integration grid (Carl Zeiss Jena GmbH, Jena, Germany) with 10 parallel lines and 100 points in a quadrangular area. The grid image was successively superimposed on approximately 13 histological fields per histological section, comprised of all tooth sockets from the coronal limit adjacent to the gingival epithelium until the lower apical limit. For each animal/socket, sections from the coronal, medial and apical thirds were evaluated. In the morphometric analysis, points were counted coinciding with the images of the following components of the alveolar socket: clot, inflammatory cells, blood vessels, fibroblasts, collagen fibers, bone matrix, osteoblasts, osteoclasts and other components (empty space left by the inflammatory exudate or intercellular liquid and bone marrow); similar to previous descriptions in other models [4,27,28]. The results were presented as the mean of volume density for each evaluated structure.

2.5. Picrosirius-polarization method

The Picrosirius-polarization method and quantification of birefringent fibers were performed to assess the structural changes in the newly formed bone trabeculae matrix based on the birefringence of the collagen fiber bundles, as previously described [29,30]. Serial sections (8 semi serial sections of each maxilla) with 5 μm thickness were cut and stained with Picrosirius Red Stain; all sections were stained simultaneously to avoid variations due to possible differences in the staining process. Picrosirius Red-stained sections were analyzed through a polarizing lens coupled to a binocular inverted microscope (Leica DM IRB/E), and all images were captured with the same parameters (the same light intensity and angle of the polarizing lens 90° to the light source). AdobePhotoshopCS6 software was used to delimit the region of interest (alveolar area comprised of new tissue with the external limit comprised of the alveolar wall). The quantification of the intensity of birefringence brightness was performed using the AxioVision 4.8 software (CarlZeiss). For quantification, the images were binarized for definition of the green, yellow and red color spectra and the quantity of each color pixels^2 corresponding to the total area enclosed in the alveoli were measured. Mean values of 4 sections from each animal were calculated in pixels^2.

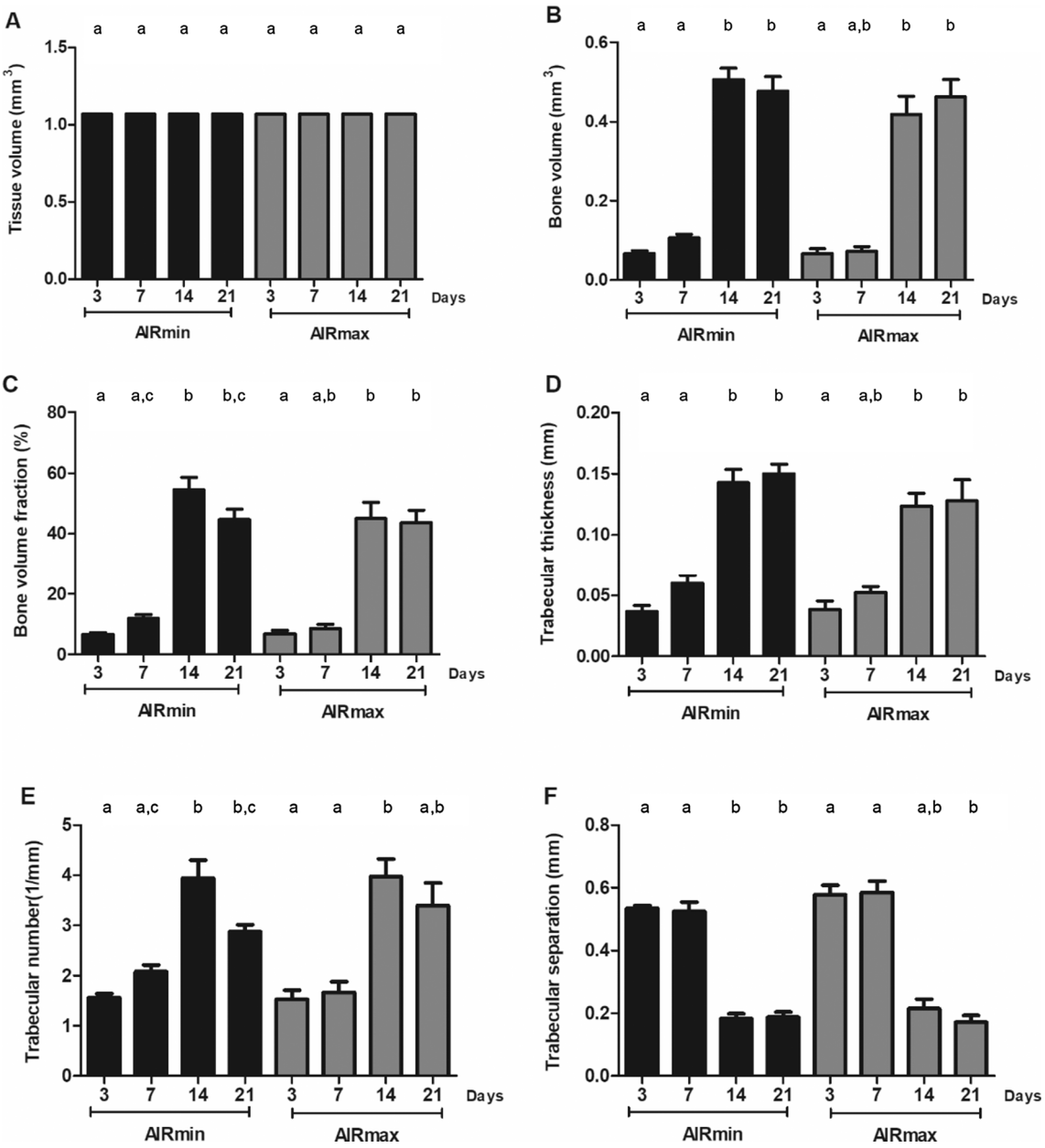

Fig. 2. Morphological parameters of the trabecular bone microarchitecture. Data were assessed using the CTAn software from the cylindrical region of interest (ROI) determined by segmenting the trabecular bone located from the coronal to apical thirds. Trabecular measurements analyzed included: (A) tissue volume (TV, mm^3), (B) bone volume (BV, mm^3), (C) bone volume fraction (BV/TV, %), (D) trabecular thickness (Tb.Th, mm), (E) trabecular number (Tb.N, 1/mm) and (F) trabecular separation (Tb.Sp, mm). Results are presented as mean (± SD). Different letters indicate significant statistical differences ($p < 0.05$) between the periods within each group; no statistically significant differences were observed upon the comparison of AIRmin and AIRmax groups in each time point.

2.6. Immunohistochemistry analysis

Histological sections from 3, 7, 14 and 21 days were deparaffinised following standard procedures. The material was pre-incubated with 3% Hydrogen Peroxidase Block (Spring Bioscience Corporation, CA, USA) and subsequently incubated with 7% NFDM to block serum proteins. The histological sections from of all groups were incubated with antibodies specific for a particular target, such as, and anti-Gr1 polyclonal antibody (sc-168490) (Santa Cruz Biotechnology, Santa Cruz, CA, USA), anti-F4/80 polyclonal antibody (sc-26642) (Santa Cruz Biotechnology, Santa Cruz, CA, USA) anti-CD80 monoclonal antibody (sc-9091) (Santa Cruz Biotechnology, Santa Cruz, CA, USA) and anti-CD206 polyclonal antibody (sc-34577) (Santa Cruz Biotechnology, Santa Cruz, CA, USA) at 1:50 concentrations for 1 h at room temperature. The identification of antigen–antibody reaction was performed using 3–3′-diaminobenzidine (DAB) and counter-staining with Mayer's hematoxylin. Positive controls were assessed in mouse spleen for positive Gr1, F4/80, CD80 and CD206 receptors. The analysis of immunolabeled cells was performed by a single calibrated investigator with a binocular light microscope (Olympus Optical Co., Tokyo, Japan) using a 100x immersion objective, and performed in a blinded way for groups and time points. The quantitative analysis for the different markers was performed throughout the alveolar extension. The absolute number of immunolabeled cells was obtained to calculate the mean for each section.

2.7. RealTime PCR array reactions

RealTimePCR array reactions were performed as previously described [31–33]. The extraction of total RNA from the remaining

Table 1
Trabecular bone microarchitecture from μCT assessment of the tooth extraction sockets along the bone healing process in AIRmin and AIRmax mice.

	AIRmin			
Parameters	3d	7d	14d	21d
BV (mm^3)	0.06 ± 0.01[a]	0.10 ± 0.02[a]	0.50 ± 0.09[b]	0.47 ± 0.11[b]
BV/TV (%)	6.62 ± 1.55[a]	11.9 ± 3.26[a,c]	54.4 ± 13.4[b]	44.6 ± 10.7[b,c]
Tb.Th (mm)	0.03 ± 0.01[a]	0.06 ± 0.01[a]	0.14 ± 0.03[b]	0.15 ± 0.02[b]
Tb.N (1/mm)	1.56 ± 0.19[a]	2.08 ± 0.36[a,c]	3.94 ± 1.19[b]	2.87 ± 0.43[b,c]
Tb.Sp (mm)	0.53 ± 0.02[a]	0.52 ± 0.08[a]	0.18 ± 0.05[b]	0.18 ± 0.05[b]
	AIRmax			
Parameters	3d	7d	14d	21d
BV (mm^3)	0.06 ± 0.02[a]	0.07 ± 0.02[a,b]	0.41 ± 0.11[b]	0.46 ± 0.09[b]
BV/TV (%)	6.74 ± 2.80[a]	8.57 ± 2.74[a,b]	45.0 ± 13.0[b]	43.6 ± 9.21[b]
Tb.Th (mm)	0.03 ± 0.01[a]	0.05 ± 0.009[a,b]	0.12 ± 0.02[b]	0.12 ± 0.03[b]
Tb.N (1/mm)	1.53 ± 0.44[a]	1.67 ± 0.41[a]	3.97 ± 0.85[b]	3.39 ± 1.00[a,b]
Tb.Sp (mm)	0.57 ± 0.07[a]	0.58 ± 0.07[a]	0.21 ± 0.07[a,b]	0.17 ± 0.04[b]

Different letters indicate significant statistical differences ($p < 0.05$) between the periods within each group.

alveolus was performed with the RNeasyFFPE kit (Qiagen Inc, Valencia, CA) according to the manufacturers' instructions. RNA samples integrity was verified by analyzing 1 μg of total RNA in a 2100 Bioanalyzer (Agilent Technologies, Santa Clara, CA) according to the manufacturers' instructions, and the complementary DNA was synthesized using 3 μg of RNA through a reverse transcription reaction (Superscript III, Invitrogen Corporation, Carlsbad, CA, USA). RealTimePCR array was performed in a Viia7 instrument (LifeTechnologies, Carlsbad, CA) using a custom panel containing targets "Wound Healing" (PAMM-121), "Inflammatory cytokines and receptors" (PAMM-011) and "Osteogenesis" (PAMM-026) (SABiosciences, Frederick, MD) for gene expression profiling. RealTimePCR array data were analyzed by the RT^2 profiler PCR Array Data Analysis online software (SABiosciences, Frederick, MD) for normalizing the initial geometric mean of three constitutive genes (GAPDH, ACTB, Hprt1) and subsequently normalized by the control group (the AIRmin and AIRmax controls mean was used as overall 'control group' for normalization), and expressed as fold change relative to the control group; as previously described [34,35].

2.8. Statistical analysis

Data were presented as means ± SD, initially the data distribution were tested by the Shapiro-Wilk normality test. Differences among data sets were statistically analyzed by ANOVA (followed by the Tukey test) or Kruskal-Wallis (followed by the Dunn's test), for the comparative analysis of the different time point in each strain, or student's *t*-test or Mann-Whitney test for the comparative analysis of AIRmin and AIRmax strains in individual time points. PCR array data were analyzed by the Mann-Whitney test followed by Benjamini-Hochberg test. Values of $p < 0.05$ were considered statistically significant. All were performed with Graph-Pad Prism 5.0 software (GraphPad Software Inc, San Diego, CA).

3. Results

3.1. Micro-computed tomography (μCT) analysis

Three-dimensional μCT analysis from the maxillae depicts the alveolar bone healing process in AIRmin and AIRmax mice over time (Fig. 1). In the initial time (0 day), in both strains the alveolus was completely void without hyperdense areas. After 3d timepoint, hyperdense areas become evident, with and evidences of centripetal bone formation from the lateral and apical walls of the extraction sockets toward the center and the coronal region of the alveolus in both strains, followed by an increase in hyperdense regions, which includes increasing trabecular number and thickness, until the endpoint, where the alveoli appears to be filled with neo formed bone, characterizing a successful healing outcome (Fig. 1) The quantitative analysis of μCT data confirms the qualitative three-dimensional analysis observations (Fig. 2). In both strains, the kinetic analysis demonstrated a progressive increase over the periods in bone volume (BV), bone volume fraction (BV/TV), trabecular thickness (Tb.Th) and trabecular number (Tb.N), along a marked reduction in trabecular separation (Tb.Sp) from 14 days (Fig. 2A–F, Table 1). However, no significant differences in the bone healing parameters between AIRmin and AIRmax strains were observed in the μCT analysis. Importantly, no significant differences were observed in healing features in males and females, used in equivalent numbers in the experiments (data not shown).

3.2. Histological, histomorphometrical and birefringence evaluation

The histological and histomorphometrical analyses was performed to the qualitative and quantitative analysis of characteristic element of distinct bone healing stages, namely blood clot, inflammatory cells, fibroblasts, collagen fibers, blood vessels, bone matrix, osteoblasts, osteoclasts and other structures; and reveals some differences between the strains (Fig. 3 and Fig. 4). Overall, the socket of both AIRmin and AIRmax strains exhibited predominantly blood clot at day 0 (immediately after tooth extraction) with a negligible number of leukocytes (Fig. 3A and B). The clot density was found to be smaller in AIRmax strain at the day 0 time point, and to be subsequently reduced over time in both strains (Fig. 4A). Additionally, we observed an abundant amount of granulation tissue (fibers, fibroblast, blood vessels and connective tissue) (Fig. 4B–E) with leucocytes infiltration at 3 days, with significant lower leukocyte counts in AIRmax strain at this time point (Fig. 4F). At 3d time point, the initial evidences of osteogenesis were detectable, with lower density of bone matrix, osteoblasts and bone tissue observed in AIRmax strain (Fig. 4G, H and J). From 7d time points, the substitution of granulation tissue by newly formed bone becomes evident, with evidences of a slight but significant delay in AIRmax strain (Fig. 3A and 3B), characterized by with lower density of bone matrix and bone tissue, and increased collagen fibers, in comparison with AIRmin strain (Fig. 4G, J and B). At 14d and 21d time points, the bone remodeling activity was evidenced by the presence of osteoclasts, which were present in a higher density in AIRmax strain (Fig. 4I). The volume density of other structures, comprised in the early times by the presence of interstitial fluid, was found to be increased in AIRmax strain at oh time point; as well be increased at 7d and 14 in this strain, when other structures are basically represented by the increased presence of bone marrow when compared to the AIRmin strain (4L). In

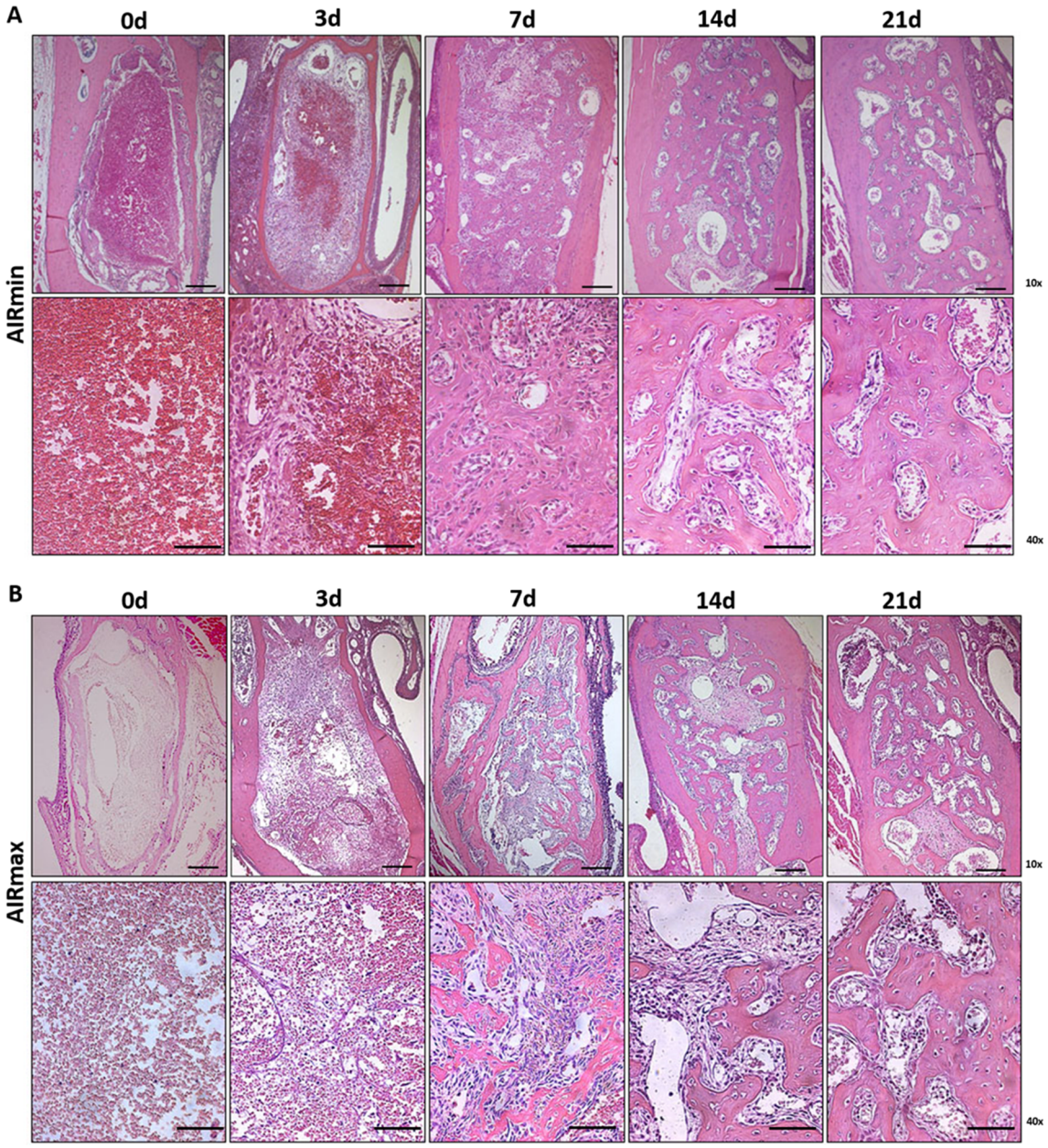

Fig. 3. Histological aspects of the medial and apical thirds from tooth sockets in the bone healing process. (A) representative sections of the alveolar bone healing kinetics at 0, 3, 7, 14 and 21 days post-extraction of the upper right incisor in AIRmin mice, as well as (B) representative sections of the alveolar bone healing in AIRmax mice. HE staining, original magnification 10x and 40x.

the birefringence analysis, the new organic matrix consisting predominantly of collagen fibers bundles were more evident after 7d time point, followed by a progressive presence in the sockets of both AIRmin and AIRmax strains, as evidenced by polarized light images (Fig. 5A and B). The quantitative analysis showed a similar pattern in the matrix maturation dynamics during the time points in both strains, characterized by the initial prevalence of collagen fibers in green tones (thinner and immature fibers) at 3d and 7d time points, followed by the prevalence of collagen fibers emitting yellow and red color spectrum (thicker and mature collagen) at the latter time points, with a decrease of in red fiber in AIRmax strain at 21d time point (Fig. 5C and D).

3.3. Immunohistochemical analysis of Gr1+, F4/80+, CD80+ and CD206+ cells

The immunohistochemical analysis was used to detect the presence of Gr1+ (granulocytes), F4/80+ (macrophages), CD80+ (M1 macrophages) and CD206+ (M2 macrophages) cells in the sites of alveolar bone repair process (Fig. 6A, 6B, 6C and 6D). The quantitative analysis of immunostained cells demonstrated higher counts of Gr1+ in AIRmax strain at 3d, while decreased counts were observed in AIRmax strain at 14d and 21d time points when compared to AIRmin (Fig. 7A). The overall counts of F4/80+ cells were similar in both strains, except for 7d time point, where AIRmin presented increased counts in comparison with AIRmax (Fig. 7B). Regarding M1 and M2 markers, CD80+ cells were presented in higher counts in AIRmax strain at 3d and 14d time points, while CD206+ cells counts were lower in AIRmax strain at 7d, when compared to AIRmin strain (Fig. 7C and D).

3.4. Molecular analysis using realtime PCRArray

Differential gene expression of several molecules involved in bone

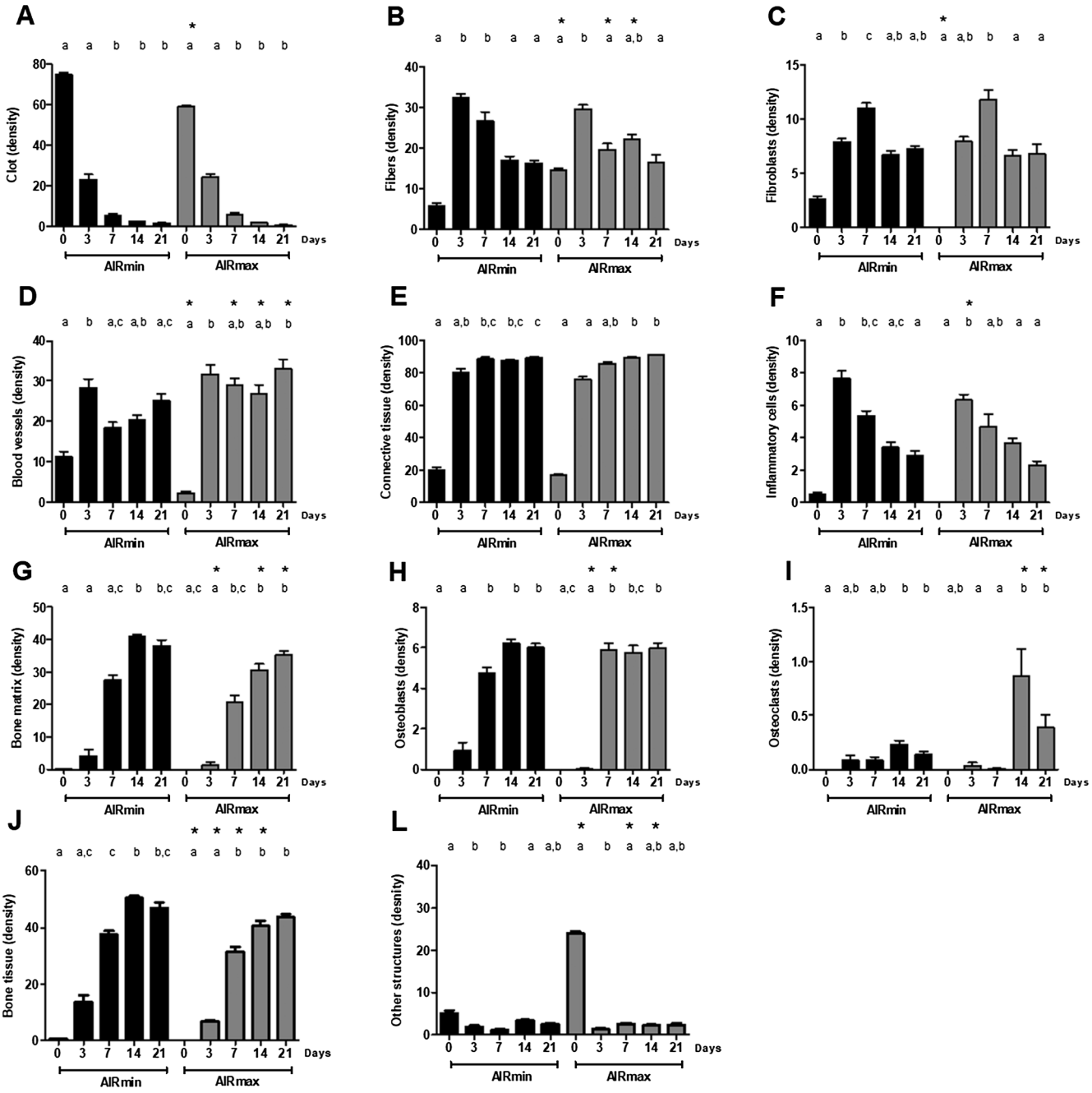

Fig. 4. Histomorphometric analysis of alveolar bone healing kinetics after tooth extraction. Results are presented as the means (± SD) of density for each structure of the alveolar socket. (A) clot, (B) fibers, (C) fibroblasts, (D) blood vessels, (E) total density of connective tissue (represented by the sum of fibers, fibroblasts, blood vessels and inflammatory cells), (F) inflammatory cells, (G) bone matrix, (H) osteoblasts, (I) osteoclasts, (J) bone tissue (represented by the sum of its structural components bone matrix, osteoblasts and osteoclasts) and (L) other components (empty space left by the inflammatory exudate or intercellular liquid). * indicates significant statistical differences ($p < 0.05$) between the AIRmin and AIRmax groups and different letters indicate significant statistical differences ($p < 0.05$) between the periods.

healing (i.e., growth factors, bone formation markers, immunological markers, and putative MSC markers) were investigated in AIRmin and AIRmax strains. An initial exploratory analysis was performed with a samples pool from all time points, and subsequently, the targets with a differential expression between AIRmin and AIRmax were analyzed in according to their kinetics of expression along all experimental periods individually. Among several growth factors, the molecules BMP4 and BMP7 expression were up regulated along bone healing in the AIRmin in comparison to AIRmax (Fig. 8A) with an expression peak at 3d and 7d (Fig. 9). VEGFA and VEGFB expression were up regulated in the AIRmax strain (Fig. 8A), with an mRNA expression peak at 7d time point (Fig. 9). Considering the inflammatory and immunological factors/markers analyzed, ARG1, CCR5, CCL5, CCL20 and CX3CL1 were upregulated in the AIRmin in comparison with AIRmax (Fig. 8A and 8B), with a peak of mRNA levels at 7 days followed by a gradual decrease in their expression in the subsequent experimental periods (Fig. 9), while IL-1β, TNF-α, CXCR1, CXCL1 and CXCL2 expression were up regulated in the AIRmax in comparison to the AIRmin (Fig. 8A and 8B), with an overall expression peak at the early experimental time points (Fig. 9). Among the extracellular matrix markers, MMP8, MMP9

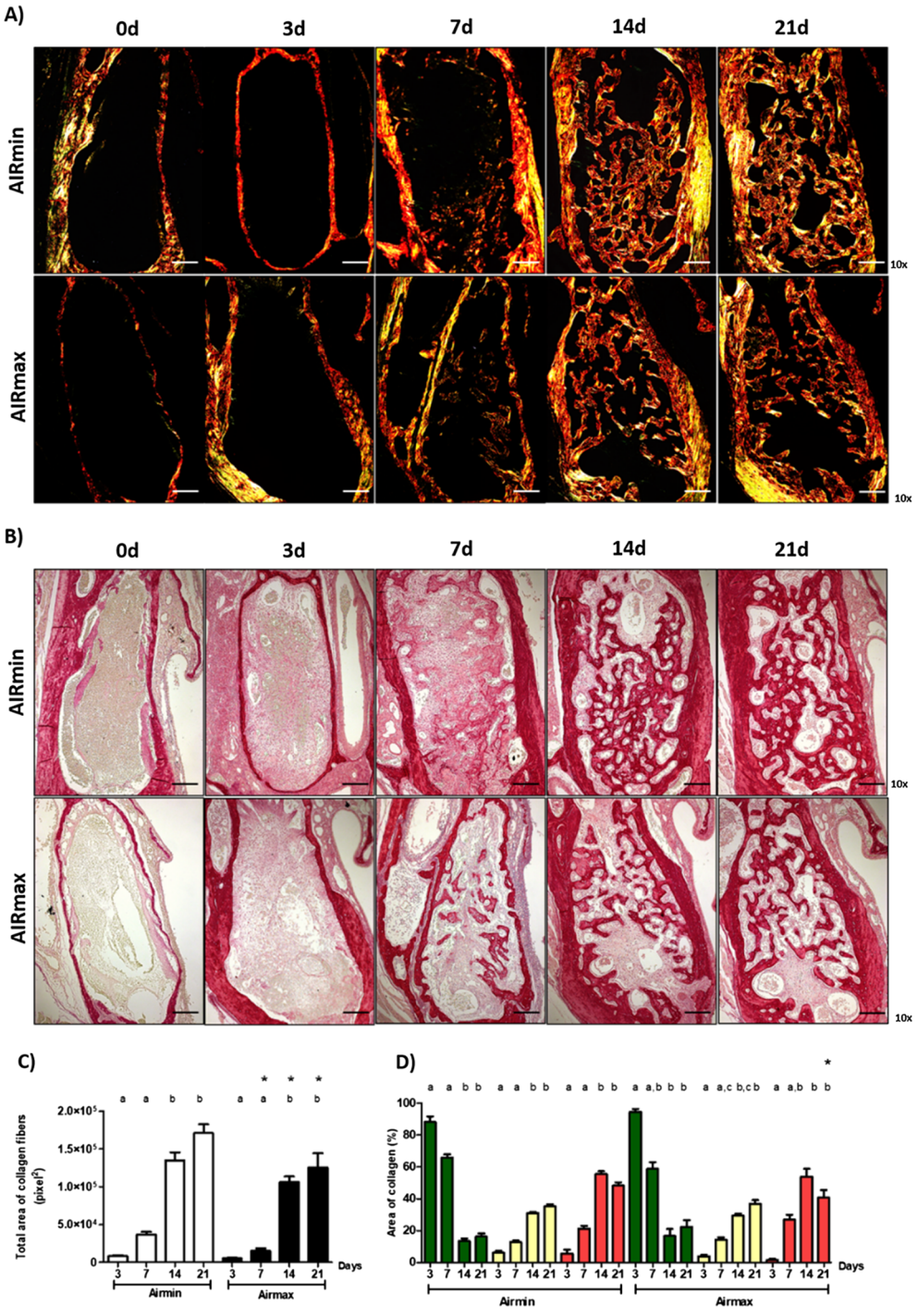

Fig. 5. Birefringence analysis of collagen fibers in the bone healing process after tooth extraction. (A and B) Representative sections of Picrosirius red staining visualized upon polarized light and conventional light to identify collagen fibers types at 0, 3, 7, 14 and 21 days. Green birefringence color indicates thin fibers; while yellow and red colors indicate thick collagen fibers. (magnification 10x and bar = 100 μm). (C) Intensity of birefringence performed using image-analysis software (AxioVision, v. 4.8, CarlZeiss) to identify and quantify: total area of collagen fibers (pixel^2), as well as (D) area of collagen from each birefringence color (pixel^2). Results are presented as mean (± SD) of pixels^2 for each color in the birefringence analysis in the bone healing at 0, 3, 7, 14 and 21 days post-extraction. * indicates significant statistical differences ($p < 0.05$) between the AIRmin and AIRmax groups and different letters indicate significant statistical differences ($p < 0.05$) between the periods. (For interpretation of the references to color in this figure legend, the reader is referred to the web version of this article.)

and MMP13 were up regulated in bone repair process in the AIRmax compared to the AIRmin (Fig. 8C), with an early expression peak for MMP8 and later expression peaks for MMP9 and MMP13 (Fig. 9). MSC marker NANOG were found positively up regulated in the AIRmin while CD34 levels were higher in AIRmax strain (Fig. 8C), both markers presented a similar expression kinetics, peaking at 7d and 14d time points (Fig. 9). Among bone markers, the early bone formation marker RUNX2 and the late bone formation markers PHEX and SOST were upregulated in the AIRmin strain (Fig. 8C), with kinetic expression patterns compatible with the early and late expression (Fig. 9). RANKL and CTSK markers were found up regulated in the AIRmax (Fig. 8C) peaking at 14d and 21d time points (Fig. 9).

4. Discussion

While a transitory and moderate host response allegedly contributes to bone healing, exacerbated responses seems to have a detrimental role in this process. However, the exact role of inflammatory immune response in bone healing process remains unclear. In this context, this study took advantage of mice strains genetically selected for maximum (AIRmax) or minimum (AIRmin) acute inflammatory response to study the relationship between contrasting inflammatory responsiveness genotypes/phenotypes and bone healing outcome. Remarkably, despite a slight, but significant, delay in the bone formation in AIRmax strain, a similar successful bone healing outcome at the endpoint was evidenced

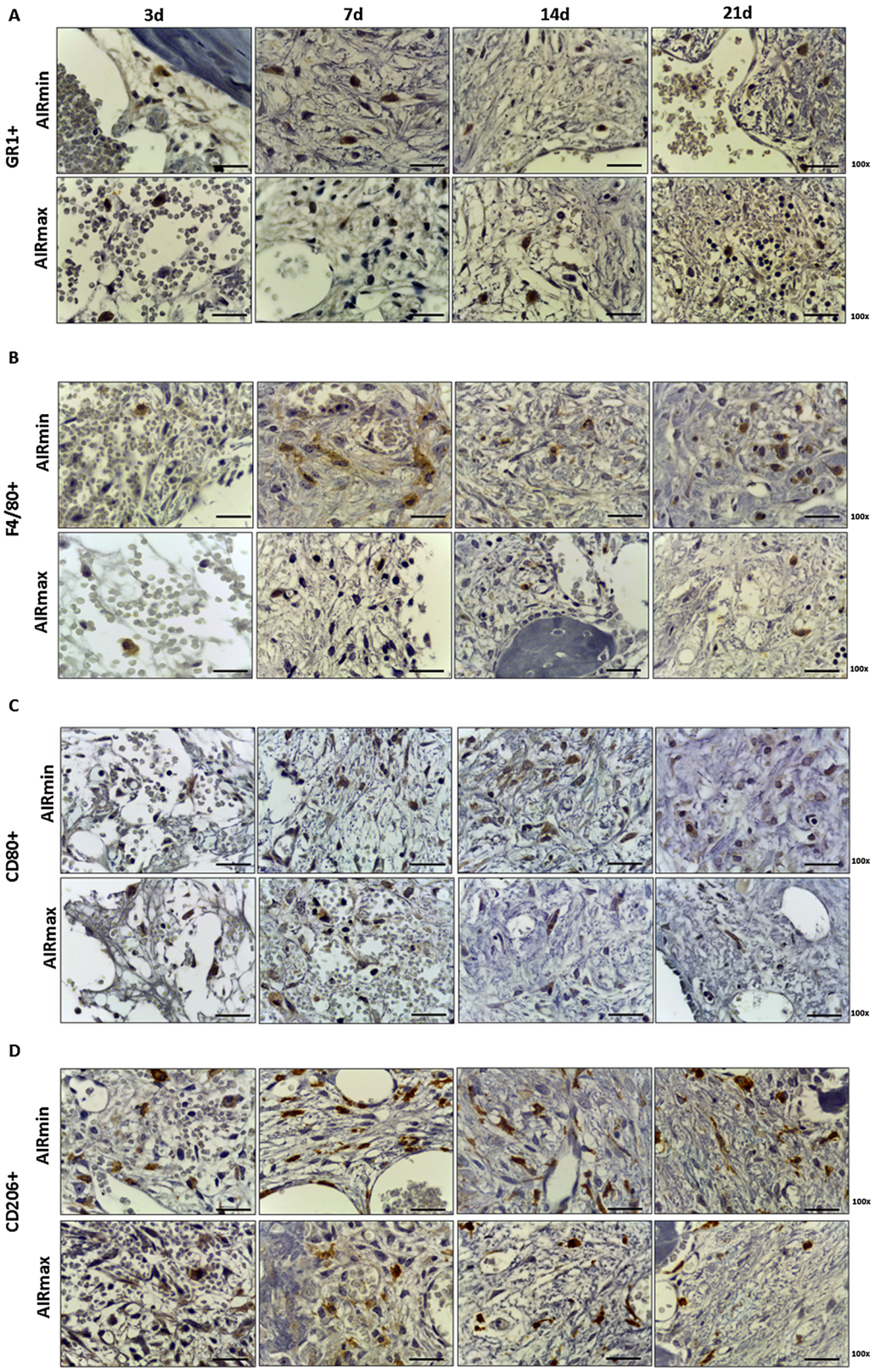

Fig. 6. Immunohistochemistry analysis for (A) GR1 +, (B) F4/80 +, (C) CD80 + and (D) CD206 + cells present in the bone repair process in the AIRmin and AIRmax mice. Representative sections from medial thirds of the socket at days 3, 7,14 and 21 days after tooth extraction. Indirect staining MACH4 + DAB, anti-staining Mayer hematoxylin; objective of 100x.

in both AIRmin and AIRmax strains, as demonstrated by microtomographic and histological/histomorphometric analysis, which similar features to that previously reported in C57Bl/6 mice [24]. However, some significant differences observed in determined time points were observed, and can provide interesting insights into the inflammation and healing interplay at alveolar area.

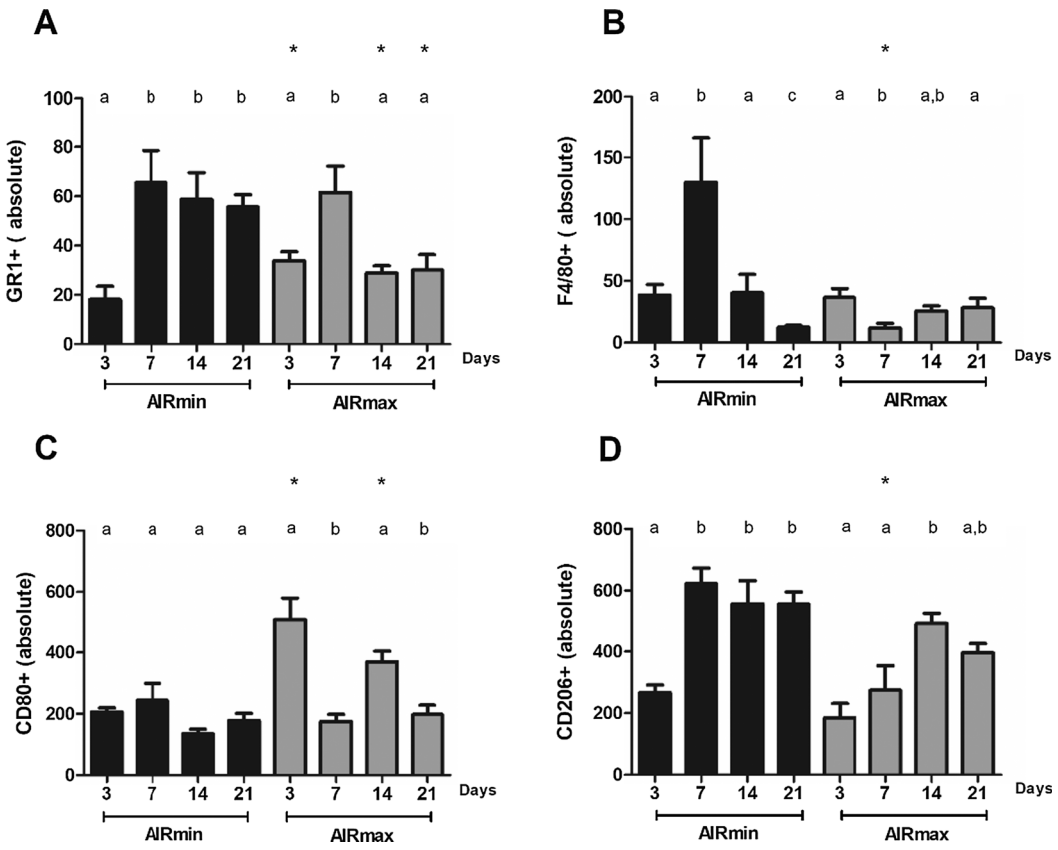

Fig. 7. Analysis of inflammatory cells in the alveolar bone healing kinetics after tooth extraction. (A) Immunohistochemistry quantification corresponding Gr1 + immunolabelled with anti-Gr1 +, (B) F4/80 + immunolabelled with anti-F4/80 +, (C) CD80 + immunolabelled with anti-CD80 + and (D) CD206 + immunolabelled with anti-CD206. Results are presented as the means (± SD) of absolute number of immunolabeled cells. * indicates significant statistical differences ($p < 0.05$) between the AIRmin and AIRmax groups and different letters indicate significant statistical differences ($p < 0.05$) between the periods.

Initially, in the view of extreme and contrasting inflammatory and healing phenotypes previously described to AIRmin and AIRmax strains [21,22], it is possible to consider that the overall similarity in bone healing outcome in these strains comprises an unpredicted phenotype. The existence of common QTLs influencing the healing processes in different tissues is supported by the description of a heritable strong genetic correlation between cartilage and ear regeneration [36]. Indeed, numerous QTLs potentially involved in soft tissue healing outcomes have been identified, including the specific QTLs underlying AIRmin and AIRmax differential healing [22,37]. However, a previous study described that intramembranous bone regeneration was largely independent of known heritable traits, including soft tissue healing [38]. In this context, it is possible to suggest that the genetic basis of intramembranous bone repair is likely distinct from the overall healing, which could account for the divergent ear and bone healing outcomes observed in AIR strains. Importantly, despite the description of genetic influence in fracture healing among different inbred mouse strains [39], and of numerous QTLs associated with bone features (i.e. composition, microarchitecture and biomechanical performance) [40–42], the QTLs associated with bone healing remain to be determined.

At this point, it is also mandatory to consider that the inflammatory phenotype observed at healing sites in the AIR strains was also unpredicted. Indeed, while AIRmin/AIRmax strains present a notable dichotomy in diverse acute and chronic inflammatory processes [17,18,43–45], similar inflammatory cell counts in the AIRmin and AIRmax strains were observed at bone healing sites. Primarily, it is necessary to consider that the nature of inflammatory process in alveolar bone healing significantly differ from the other models where AIRmin/AIRmax strains were investigated. Alveolar bone healing comprise an 'sterile' inflammation process, being the inflammatory response theoretically triggered by DAMPs derived from tissue damage [24]. Also, alveolar bone healing requires a major clotting process to fulfill the alveolar socket; followed by a transitory inflammatory reaction and of the formation of granulation tissue [24]. Such transitional tissue, upon inflammation resolution evolves to a newly formed bone tissue [24]. Importantly, the 'AIR' genotypes/phenotypes selection was based in leukocyte and serum protein accumulation in the exudate in response to a neutral substrate (suspension of polyacrylamide microbeads) in the subcutaneous compartment [18]. Additionally, the infectious and chronic inflammation models which replicates opposing minimal and maximal inflammatory phenotypes [17,18,43–45] also clearly differ from the bone healing scenario, where the inflammatory response is supposedly triggered by DAMPs in a different cellular environment.

Therefore, it is plausible that different QTLs may control the inflammatory responsiveness in different contexts, i.e. involving distinct stimuli and different tissues. Indeed, QTLs on chromosomes 12 and 16 are suggested to modulate development and resolution of sterile inflammation in AXB-BXA RI strains [46], while QTLs chromosomes 1 and 14 are associated with AIRmin/AIRmax inflammatory and healing capacity [18,23]. It is also important to understand the complexity of the genetic influence in complex multi-stage processes such as ear or bone healing. Indeed, individual QTLs can modulate specific stages and/or events involved in healing, such as clotting [47], early inflammatory events [21], angiogenesis [48], collagen production [49,50], tissue mineralization [51]. The existence of multiple putative 'QTL control points' highlights the complexity of genetic network underlying bone healing outcome. Indeed, genetic control of inflammatory and healing phenotypes in AIR strains involves diverse QTLs and specific genes/alleles, such as *Slc11a1* [21], which account

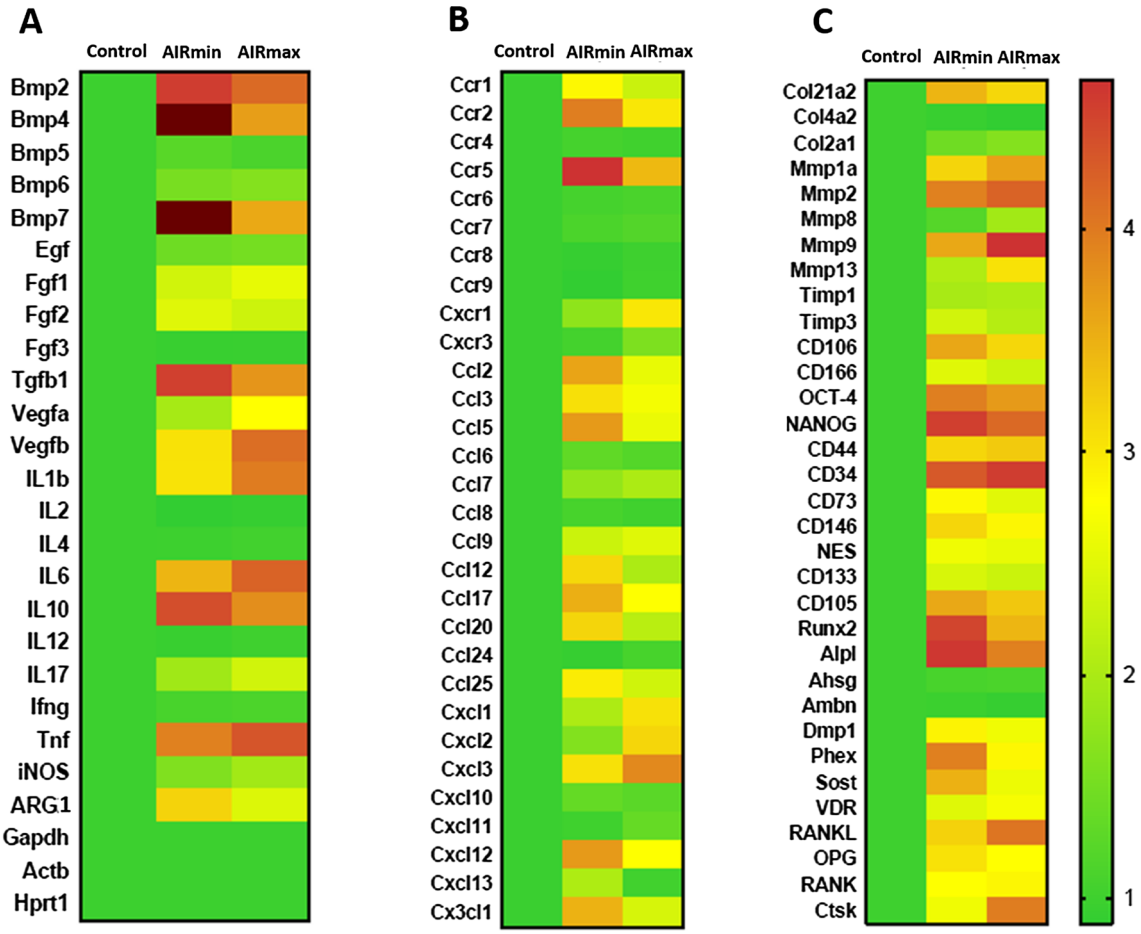

Fig. 8. Molecular analysis (PCRArray) using Heat map to quantify the expression of (A) growth factors and cytokine markers, (B) extracellular matrix markers and (C) bone markers in bone healing process among AIRmin and AIRmax, post tooth extraction. PCRArray of pooled samples. Results were obtained when comparing the relative expression of the different groups to the normalizing control.

for a significant extent for the differential response between the strains [22]. *Slc11a1* alleles are named *R* or *S* once they confer resistance (R) or susceptibility (S) to a series of infectious conditions [52,53]. In fact, subsequent studies have demonstrated significant frequency differences on these alleles in the AIRmax and AIRmin strains, the *R* allele being predominate AIRmax animals, while the presence of the allele *S* is characteristic of the AIRmin strain [52].

However, despite similar healing outcome, AIRmin and AIRmax strains presents some significant differences in bone healing kinetics/stages which can provide interesting insights into the inflammation/healing relationship. Initially, the histormophometric analysis reveal a slight but significant delay in the bone formation in the early times in AIRmax strain when compared with AIRmin counterpart. Accordingly, such alteration was accompanied by a decreased expression of BMP2, BMP4, BMP7 and TGFb1, collectively responsible by osteoblastic differentiation, RUNX2, the master transcription factor responsible for osteoblastic phenotype acquisition, and ALP, a key enzyme of bone mineralization process [54–57].

Looking for possible reasons underlying the initial delay in bone formation in AIRmax strain, a decrease in blood clot and inflammatory cell density were also observed in the early times when compared with AIRmin strain. Accordingly, the clotting process is classically described as an essential element of alveolar healing [9].The proper clot formation allows the subsequent recruitment of different inflammatory cell subsets, which is a key step of healing process [58]. Interestingly, while the histomorphometric analysis reveals an overall quantitative similarity in the inflammatory infiltrate, the nature of the cells comprising the inflammatory infiltrate differ between AIRmin and AIRmax strains.

Initially, it becomes evident the initial predominance of neutrophils (i.e.GR1 + cells) in the initial inflammatory response in AIRmax strain, in parallel with increased levels of CXCL1 and CXCL2, and its receptor CXCR1. Accordingly, CXCL1 and CLXCL2 exerts a major role in neutrophil chemoattraction via CXCR1 [52]. Previous studies describe that AIRmax mice features a higher neutrophil production in the bone medulla, a higher concentration of neutrophils in blood and an increased resistance of locally infiltrated neutrophils to spontaneous apoptosis [44,53], which could also contribute to the increased neutrophil infiltration. A recent study describe that neutrophil recruitment is essential to create an provisional extracellular matrix and initiate downstream responses that mediate bone fracture healing [59,60]. However, neutrophils inhibit the synthesis of mineralized extracellular matrix [61], which could account for the delayed repair in AIRmax strain due increased neutrophil counts and activity. It is necessary to consider that the proper repair observed in AIRmin strain was associated with increased neutrophil counts in the latter stages, which add some complexity to the neutrophils/healing interplay. One possible explanation refers to the relatively recent description of neutrophils N1 and N2 subsets [62], which could account for distinct outcomes of healing [63]. However, neutrophils subsets are still unclear, and further studies are required to explore its potential modulation of healing stages.

Regarding the putative influence of macrophages subsets in bone healing, M2 macrophages (i.e CD206 + cells) are in relative predominance in AIRmin strain, while M1 macrophages (i.e CD80 + cells)

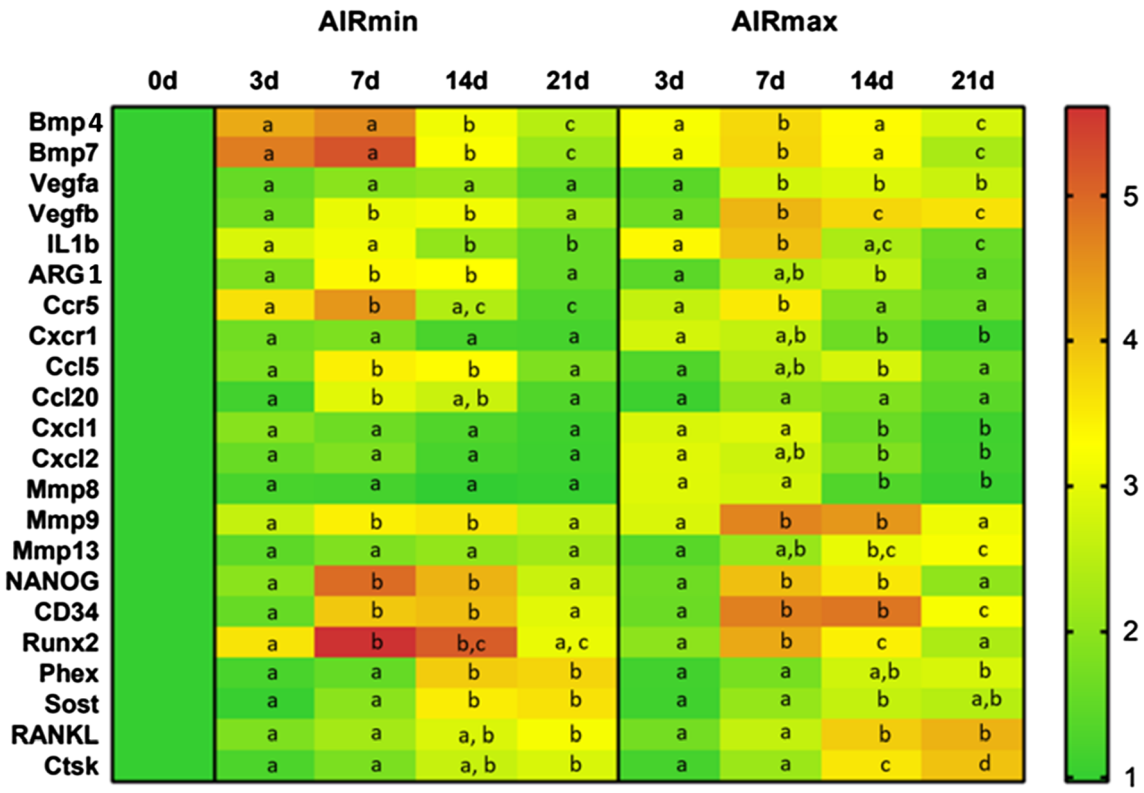

Fig. 9. Molecular analysis (PCRArray) using Heat map to quantify the expression of the growth factors, extracellular matrix, bone markers and cytokines markers in bone healing process among AIRmin and AIRmax, post tooth extraction. PCRArray of pooled samples at different periods. Results were obtained when comparing the relative expression of the different groups to the normalizing control, thus, lowercase letters represent statistically significant difference ($p < 0.05$) between indicated groups.

prevail in AIRmax. Macrophages polarized into a M1 phenotype are considered pro-inflammatory cells, being able to produce high levels of pro-inflammatory cytokines like TNF and IL-6, and iNOS [64]. Conversely, M2 macrophages are characterized by high expression of anti-inflammatory and pro-reparative/anabolic cytokines such as IL-10 and TGFβ1, as well as ARG-1 [65–67]. Accordingly, the molecular analysis demonstrated increased levels of M2 markers (ARG1, IL-10, TGFb) in AIRmin strain, while pro-inflammatory M1-related factors (IL1B, IL6, TNF) prevail in AIRmax strain. While the initial M1 macrophages has been implicated as essential for activation of acute inflammatory response, M2 cells are considered favorable for regenerative outcome [68–72]. Indeed, previous studies demonstrate that the repair process involves an initial M1 polarization that rapidly evolves to M2 [73]. In this context, the initial M1/M2 imbalance in AIRmax strain could account for the bone healing delay observed. It is also important to mention that the F4/80+ cells counts in AIRmin outnumber those observed in AIRmax healing sites. Such data reinforces the potential involvement of macrophages in the bone healing, since these cells undergo its polarization towards a proper phenotype [74]. Accordingly, the increased macrophage migration is supported by the expression of the chemokines CCL2 and CCL5, and the chemokine receptors CCR2 and CCR5, characteristically involved in macrophages chemotaxis [75].

Finally, when comparing the later healing stages between the AIR strains, we observed evidences of a larger bone remodeling in AIRmax strain, characterized by increased density of blood vessels, osteoclasts in parallel with decreased bone matrix density. Accordingly, AIRmax healing sites presents increased levels of angiogenesis- (VEGFA and VEGFB) and osteoclasts- (RANKL, CATEPk) –related factors, characteristic markers of bone remodeling and osteoclastic activity [76,77]. Interestingly, an increased M1/M2 ratio was described to contribute to osteoclastogenesis [68,78], which also could rationalize the increased osteoclasts counts in AIRmax strain. Interestingly, a regulatory feedback mechanism was recently described, where osteoclasts suppress M1 state via oc-stamp [79]. Therefore, it is possible to assume the existence of a complex regulatory pathway operating in bone healing sites, where the initially increased M1/M2 ratio boosts osteoclastogenesis, and is subsequently a target of the regulatory loop. Also, healing sites of AIRmax strain presented lower levels of mature bone makers PHEX and SOST [24], which support the evidence of the increased remodeling activity. The increased remodeling activity is also supported by the decrease of mature (red birefringent) fibers, and increased expression of MMP2, MMP8 and MMM13 in AIRmax strain. Accordingly, MMPs are important for the migration of inflammatory cells, degradation and remodeling of the extracellular matrix proteins and in the angiogenesis processes [80–82].

5. Conclusion

In summary, the present study demonstrated an overall similar inflammatory response at healing sites and similar healing outcome in AIRmin and AIRmax strains. In the view of contrasting inflammatory and healing phenotypes of AIRmin and AIRmax strains in other models, the unpredicted phenotype observed suggests the existence of specific QTLs responsible for bone healing, as well for the regulation of 'sterile' inflammation process that takes place as an initial step of bone healing events. Despite the similar endpoint healing, our results demonstrate that the delayed repair observed in the AIRmax strain was associated with increased presence of neutrophils and M1 macrophages, supporting the association of M2 cells with faster bone healing. Further studies are required to clarify the elements responsible for the regulation of inflammatory events at bone healing sites, as well the determinants of bone healing outcome.

Acknowledgements

The authors thank Daniele Ceolin, Patricia Germino, and Tania Cestari for their excellent technical assistance.

Funding

This work was supported by grants and scholarships from São Paulo Research Foundation, FAPESP (2013/25824-6 and 2015/24637-3), CNPq and CAPES. GPG and MDF receive Scientific Research productivity fellowships from CNPq.

Conflict of interest

The authors deny any conflicts of interest related to this study.

References

[1] H.K. Datta, W.F. Ng, J.A. Walker, S.P. Tuck, S.S. Varanasi, The cell biology of bone metabolism, J. Clin. Pathol. 61 (5) (2008) 577–587.
[2] R. Dimitriou, E. Tsiridis, P.V. Giannoudis, Current concepts of molecular aspects of bone healing, Injury 36 (12) (2005) 1392–1404.
[3] L.T. Duong, G.A. Rodan, Regulation of osteoclast formation and function, Rev. Endocr. Metab. Disord. 2 (1) (2001) 95–104.
[4] M.T. Rodrigues, C.L. Cardoso, P.S. Carvalho, T.M. Cestari, M. Feres, G.P. Garlet, O. Ferreira Jr., Experimental alveolitis in rats: microbiological, acute phase response and histometric characterization of delayed alveolar healing, J. Appl. Oral. Sci. 19 (3) (2011) 260–268.
[5] K. Schmidt-Bleek, H. Schell, J. Lienau, N. Schulz, P. Hoff, M. Pfaff, G. Schmidt, C. Martin, C. Perka, F. Buttgereit, H.D. Volk, G. Duda, Initial immune reaction and angiogenesis in bone healing, J. Tissue Eng. Regen. Med. 8 (2) (2014) 120–130.
[6] G.P. Garlet, W.V. Giannobile, Macrophages: The Bridge between Inflammation Resolution and Tissue Repair? J. Dent. Res. 97 (10) (2018) 1079–1081.
[7] S.A. Eming, M. Hammerschmidt, T. Krieg, A. Roers, Interrelation of immunity and tissue repair or regeneration, Semin. Cell Dev. Biol. 20 (5) (2009) 517–527.
[8] G.P. Garlet, The journal of applied oral science and the open science era, J. Appl. Oral. Sci. 21 (1) (2013).
[9] I. Konnecke, A. Serra, T. El Khassawna, C. Schlundt, H. Schell, A. Hauser, A. Ellinghaus, H.D. Volk, A. Radbruch, G.N. Duda, K. Schmidt-Bleek, T and B cells participate in bone repair by infiltrating the fracture callus in a two-wave fashion, Bone 64 (2014) 155–165.
[10] C.C. Biguetti, A.E. Vieira, F. Cavalla, A.C. Fonseca, P.M. Colavite, R.M. Silva, A.P.F. Trombone, G.P. Garlet, CCR2 Contributes to F4/80+ cells migration along intramembranous bone healing in maxilla, but its deficiency does not critically affect the healing outcome, Front Immunol. 9 (2018) 1804.
[11] H. Takayanagi, Osteoimmunology: shared mechanisms and crosstalk between the immune and bone systems, Nat. Rev. Immunol 7 (4) (2007) 292–304.
[12] J. Caetano-Lopes, H. Canhao, J.E. Fonseca, Osteoimmunology–the hidden immune regulation of bone, Autoimmun. Rev. 8 (3) (2009) 250–255.
[13] G.P. Garlet, Destructive and protective roles of cytokines in periodontitis: a re-appraisal from host defense and tissue destruction viewpoints, J. Dent. Res. 89 (12) (2010) 1349–1363.
[14] H. Takayanagi, Inflammatory bone destruction and osteoimmunology, J. Periodontal Res. 40 (4) (2005) 287–293.
[15] G.P. Garlet, C.R. Cardoso, A.P. Campanelli, T.P. Garlet, M.J. Avila-Campos, F.Q. Cunha, J.S. Silva, The essential role of IFN-gamma in the control of lethal Aggregatibacter actinomycetemcomitans infection in mice, Microbes Infect. 10 (5) (2008) 489–496.
[16] T.P. Garlet, S.Y. Fukada, I.F. Saconato, M.J. Avila-Campos, T.A. da Silva, G.P. Garlet, Q. Cunha Fde, CCR2 deficiency results in increased osteolysis in experimental periapical lesions in mice, J. Endod. 36 (2) (2010) 244–250.
[17] A.P. Trombone, M. Claudino, P. Colavite, G.F. de Assis, M.J. Avila-Campos, J.S. Silva, A.P. Campanelli, O.M. Ibanez, M. De Franco, G.P. Garlet, Periodontitis and arthritis interaction in mice involves a shared hyper-inflammatory genotype and functional immunological interferences, Genes Immun. 11 (6) (2010) 479–489.
[18] O.M. Ibanez, C. Stiffel, O.G. Ribeiro, W.K. Cabrera, S. Massa, M. de Franco, O.A. Sant'Anna, C. Decreusefond, D. Mouton, M. Siqueira, et al., Genetics of non-specific immunity: I Bidirectional selective breeding of lines of mice endowed with maximal or minimal inflammatory responsiveness, Eur. J. Immunol. 22 (10) (1992) 2555–2563.
[19] L.C. Peters, J.R. Jensen, A. Borrego, W.H. Cabrera, N. Baker, N. Starobinas, O.G. Ribeiro, O.M. Ibanez, M. De Franco, Slc11a1 (formerly NRAMP1) gene modulates both acute inflammatory reactions and pristane-induced arthritis in mice, Genes Immun. 8 (1) (2007) 51–56.
[20] G. Biozzi, O.G. Ribeiro, A. Saran, M.L. Araujo, D.A. Maria, M. De Franco, W.K. Cabrera, O.A. Sant'anna, S. Massa, V. Covelli, D. Mouton, T. Neveu, M. Siqueira, O.M. Ibanez, Effect of genetic modification of acute inflammatory responsiveness on tumorigenesis in the mouse, Carcinogenesis 19 (2) (1998) 337–346.
[21] T. Canhamero, B. Reines, L.C. Peters, A. Borrego, P.S. Carneiro, L.L. Albuquerque, W.H. Cabrera, O.G. Ribeiro, J.R. Jensen, N. Starobinas, O.M. Ibanez, M. De Franco, Distinct early inflammatory events during ear tissue regeneration in mice selected for high inflammation bearing Slc11a1 R and S alleles, Inflammation 34 (5) (2011) 303–313.
[22] T. Canhamero, L.V. Garcia, M. De Franco, Acute inflammation loci are involved in wound healing in the mouse ear punch model, Adv. Wound Care (New Rochelle) 3 (9) (2014) 582–591.
[23] M. De Franco, S. Carneiro Pdos, L.C. Peters, F. Vorraro, A. Borrego, O.G. Ribeiro, N. Starobinas, W.K. Cabrera, O.M. Ibanez, Slc11a1 (Nramp1) alleles interact with acute inflammation loci to modulate wound-healing traits in mice, Mamm Genome 18 (4) (2007) 263–269.
[24] A.E. Vieira, C.E. Repeke, B. Ferreira Junior Sde, P.M. Colavite, C.C. Biguetti, R.C. Oliveira, G.F. Assis, R. Taga, A.P. Trombone, G.P. Garlet, Intramembranous bone healing process subsequent to tooth extraction in mice: micro-computed tomography, histomorphometric and molecular characterization, PLoS One 10 (5) (2015).
[25] M.L. Bouxsein, S.K. Boyd, B.A. Christiansen, R.E. Guldberg, K.J. Jepsen, R. Muller, Guidelines for assessment of bone microstructure in rodents using micro-computed tomography, J. Bone Miner. Res. 25 (7) (2010) 1468–1486.
[26] S. Kuroshima, B.L. Kovacic, K.M. Kozloff, L.K. McCauley, J. Yamashita, Intra-oral PTH administration promotes tooth extraction socket healing, J. Dent. Res. 92 (6) (2013) 553–559.
[27] C.L. Cardoso, O. Ferreira Junior, P.S. Carvalho, T.J. Dionisio, T.M. Cestari, G.P. Garlet, Experimental dry socket: microscopic and molecular evaluation of two treatment modalities, Acta Cir. Bras. 26 (5) (2011) 365–372.
[28] A. Scala, N.P. Lang, M.T. Schweikert, J.A. de Oliveira, I. Rangel-Garcia Jr., D. Botticelli, Sequential healing of open extraction sockets. An experimental study in monkeys, Clin. Oral. Implants Res. 25 (3) (2014) 288–295.
[29] P.S. Bossini, A.C. Renno, D.A. Ribeiro, R. Fangel, A.C. Ribeiro, A. Lahoz Mde, N.A. Parizotto, Lowlevel laser therapy (830nm) improves bone repair in osteoporotic rats: similar outcomes at two different dosages, Exp. Gerontol. 47 (2) (2012) 136–142.
[30] I. Garavello-Freitas, V. Baranauskas, P.P. Joazeiro, C.R. Padovani, M. Dal Pai-Silva, M.A. da Cruz-Hofling, Low-power laser irradiation improves histomorphometrical parameters and bone matrix organization during tibia wound healing in rats, J. Photochem. Photobiol. B 70 (2) (2003) 81–89.
[31] A.C. Araujo-Pires, C.C. Biguetti, C.E. Repeke, O. Rodini Cde, A.P. Campanelli, A.P. Trombone, A. Letra, R.M. Silva, G.P. Garlet, Mesenchymal stem cells as active prohealing and immunosuppressive agents in periapical environment: evidence from human and experimental periapical lesions, J. Endod. 40 (10) (2014) 1560–1565.
[32] A.C. Araujo-Pires, A.E. Vieira, C.F. Francisconi, C.C. Biguetti, A. Glowacki, S. Yoshizawa, A.P. Campanelli, A.P. Trombone, C.S. Sfeir, S.R. Little, G.P. Garlet, IL-4/CCL22/CCR4 axis controls regulatory T-cell migration that suppresses inflammatory bone loss in murine experimental periodontitis, J. Bone Miner. Res. 30 (3) (2015) 412–422.
[33] A.J. Glowacki, S. Yoshizawa, S. Jhunjhunwala, A.E. Vieira, G.P. Garlet, C. Sfeir, S.R. Little, Prevention of inflammation-mediated bone loss in murine and canine periodontal disease via recruitment of regulatory lymphocytes, Proc. Natl. Acad. Sci. U S A 110 (46) (2013) 18525–18530.
[34] K. Campos, C.F. Franscisconi, V. Okehie, L.C. de Souza, A.P. Trombone, A. Letra, G.P. Garlet, R.S. Gomez, R.M. Silva, FOXP3 DNA methylation levels as a potential biomarker in the development of periapical lesions, J. Endod. 41 (2) (2015) 212–218.
[35] G.P. Garlet, R. Horwat, H.L. Ray Jr., T.P. Garlet, E.M. Silveira, A.P. Campanelli, A.P. Trombone, A. Letra, R.M. Silva, Expression analysis of wound healing genes in human periapical granulomas of progressive and stable nature, J. Endod. 38 (2) (2012) 185–190.
[36] M.F. Rai, S. Hashimoto, E.E. Johnson, K.L. Janiszak, J. Fitzgerald, E. Heber-Katz, J.M. Cheverud, L.J. Sandell, Heritability of articular cartilage regeneration and its association with ear wound healing in mice, Arthritis Rheum. 64 (7) (2012) 2300–2310.
[37] J.M. Cheverud, H.A. Lawson, R. Funk, J. Zhou, E.P. Blankenhorn, E. Heber-Katz, Healing quantitative trait loci in a combined cross analysis using related mouse strain crosses, Heredity (Edinb) 108 (4) (2012) 441–446.
[38] M.M. Moran, A.S. Virdi, K. Sena, S.R. Mazzone, M.A. McNulty, D.R. Sumner, Intramembranous bone regeneration differs among common inbred mouse strains following marrow ablation, J. Orthop. Res. 33 (9) (2015) 1374–1381.
[39] M.B. Manigrasso, J.P. O'Connor, Comparison of fracture healing among different inbred mouse strains, Calcif. Tissue Int. 82 (6) (2008) 465–474.
[40] J. Kristianto, S.J. Litscher, M.G. Johnson, F. Patel, M. Patel, J. Fisher, R.K. Zastrow, A.B. Radcliff, R.D. Blank, Congenic strains confirm the pleiotropic effect of chromosome 4 QTL on mouse femoral geometry and biomechanical performance, PLoS One 11 (2) (2016) e0148571.
[41] K.S. Mader, L.R. Donahue, R. Muller, M. Stampanoni, High-throughput phenotyping and genetic linkage of cortical bone microstructure in the mouse, BMC Genomics 16 (2015) 493.
[42] O.L. Sabik, J.F. Medrano, C.R. Farber, Genetic dissection of a QTL affecting, Bone Geometry, G3 (Bethesda) 7 (3) (2017) 865–870.
[43] A.S. Carneiro, O.G. Ribeiro, M. De Franco, W.H. Cabrera, F. Vorraro, M. Siqueira, O.M. Ibanez, N. Starobinas, Local inflammatory reaction induced by Bothrops jararaca venom differs in mice selected for acute inflammatory response, Toxicon 40 (11) (2002) 1571–1579.
[44] J.G. Fernandes, T. Canhamero, A. Borrego, J.R. Jensen, W.H. Cabrera, M.A. Correa, N. Starobinas, O.G. Ribeiro, O.M. Ibanez, M. De Franco, Distinct gene expression profiles provoked by polyacrylamide beads (Biogel) during chronic and acute

inflammation in mice selected for maximal and minimal inflammatory responses, Inflamm. Res. 65 (4) (2016) 313–323.
[45] A.P. Trombone, S.B. Ferreira Jr., F.M. Raimundo, K.C. de Moura, M.J. Avila-Campos, J.S. Silva, A.P. Campanelli, M. De Franco, G.P. Garlet, Experimental periodontitis in mice selected for maximal or minimal inflammatory reactions: increased inflammatory immune responsiveness drives increased alveolar bone loss without enhancing the control of periodontal infection, J. Periodontal Res. 44 (4) (2009) 443–451.
[46] Q. Cheng, Z. Seltzer, C. Sima, F.S. Lakschevitz, M. Glogauer, Quantitative trait loci and candidate genes for neutrophil recruitment in sterile inflammation mapped in AXB-BXA recombinant inbred mice, PLoS One 10 (5) (2015) e0124117.
[47] J. Hoover-Plow, Q. Sa, M. Huang, J. Grondolsky, Genetic dissection of quantitative trait Loci for hemostasis and thrombosis on mouse chromosomes 11 and 5 using congenic and subcongenic strains, PLoS One 8 (10) (2013) e77539.
[48] K. Morales, L. Rowehl, J. Smith, R. Cole, F. Liu, B. Beyer, B.J. Herron, Mapping novel subcutaneous angiogenesis quantitative trait loci in [B6xMRL]F2 mice, Adv. Wound Care (New Rochelle) 3 (9) (2014) 563–572.
[49] R.A. Hall, S. Hillebrandt, F. Lammert, Exploring multiple quantitative trait loci models of hepatic fibrosis in a mouse intercross, Mamm. Genome. 27 (1–2) (2016) 70–80.
[50] N. Kato, Y. Watanabe, Y. Ohno, T. Inoue, Y. Kanno, H. Suzuki, H. Okada, Mapping quantitative trait loci for proteinuria-induced renal collagen deposition, Kidney Int. 73 (9) (2008) 1017–1023.
[51] M.F. Rai, E.J. Schmidt, S. Hashimoto, J.M. Cheverud, L.J. Sandell, Genetic loci that regulate ectopic calcification in response to knee trauma in LG/J by SM/J advanced intercross mice, J. Orthop. Res. 33 (10) (2015) 1412–1423.
[52] L.M. Araujo, O.G. Ribeiro, M. Siqueira, M. De Franco, N. Starobinas, S. Massa, W.H. Cabrera, D. Mouton, M. Seman, O.M. Ibanez, Innate resistance to infection by intracellular bacterial pathogens differs in mice selected for maximal or minimal acute inflammatory response, Eur. J. Immunol. 28 (9) (1998) 2913–2920.
[53] O.G. Ribeiro, D.A. Maria, S. Adriouch, S. Pechberty, W.H. Cabrera, J. Morisset, O.M. Ibanez, M. Seman, Convergent alteration of granulopoiesis, chemotactic activity, and neutrophil apoptosis during mouse selection for high acute inflammatory response, J. Leukoc. Biol. 74 (4) (2003) 497–506.
[54] A. Bandyopadhyay, K. Tsuji, K. Cox, B.D. Harfe, V. Rosen, C.J. Tabin, Genetic analysis of the roles of BMP2, BMP4, and BMP7 in limb patterning and skeletogenesis, PLoS Genet. 2 (12) (2006) e216.
[55] R.T. Franceschi, G. Xiao, D. Jiang, R. Gopalakrishnan, S. Yang, E. Reith, Multiple signaling pathways converge on the Cbfa1/Runx2 transcription factor to regulate osteoblast differentiation, Connect. Tissue Res. 44 (Suppl 1) (2003) 109–116.
[56] V. Goriainov, R. Cook, M.L. J, G.D. D, R.O. Oreffo, Bone and metal: an orthopaedic perspective on osseointegration of metals, Acta Biomater. 10 (10) (2014) 4043–4057.
[57] J.R. Lieberman, A. Daluiski, T.A. Einhorn, The role of growth factors in the repair of bone. Biology and clinical applications, J. Bone Joint Surg. Am. 84 (A(6)) (2002) 1032–1044.
[58] T.A. Einhorn, L.C. Gerstenfeld, Fracture healing: mechanisms and interventions, Nat. Rev.Rheumatol 11 (1) (2015) 45–54.
[59] O.W. Bastian, L. Koenderman, J. Alblas, L.P. Leenen, T.J. Blokhuis, Neutrophils contribute to fracture healing by synthesizing fibronectin+ extracellular matrix rapidly after injury, Clin. Immunol. 164 (2016) 78–84.
[60] A. Kovtun, S. Bergdolt, R. Wiegner, P. Radermacher, M. Huber-Lang, A. Ignatius, The crucial role of neutrophil granulocytes in bone fracture healing, Eur. Cell Mater. 32 (2016) 152–162.
[61] O.W. Bastian, M. Croes, J. Alblas, L. Koenderman, L.P.H. Leenen, T.J. Blokhuis, Neutrophils inhibit synthesis of mineralized extracellular matrix by human bone marrow-derived stromal cells In Vitro, Front Immunol. 9 (2018) 945.
[62] Z.G. Fridlender, J. Sun, S. Kim, V. Kapoor, G. Cheng, L. Ling, G.S. Worthen, S.M. Albelda, Polarization of tumor-associated neutrophil phenotype by TGF-beta: "N1" versus "N2" TAN, Cancer Cell 16 (3) (2009) 183–194.
[63] Y. Ma, A. Yabluchanskiy, R.P. Iyer, P.L. Cannon, E.R. Flynn, M. Jung, J. Henry, C.A. Cates, K.Y. Deleon-Pennell, M.L. Lindsey, Temporal neutrophil polarization following myocardial infarction, Cardiovasc Res 110 (1) (2016) 51–61.
[64] K. Pappas, A.I. Papaioannou, K. Kostikas, N. Tzanakis, The role of macrophages in obstructive airways disease: chronic obstructive pulmonary disease and asthma, Cytokine 64 (3) (2013) 613–625.
[65] S. Bashir, Y. Sharma, A. Elahi, F. Khan, Macrophage polarization: the link between inflammation and related diseases, Inflamm. Res. 65 (1) (2016) 1–11.
[66] D.A. Hume, The many alternative faces of macrophage activation, Front Immunol. 6 (2015) 370.
[67] M.P. Motwani, D.W. Gilroy, Macrophage development and polarization in chronic inflammation, Semin. Immunol. 27 (4) (2015) 257–266.
[68] D. He, X. Kou, Q. Luo, R. Yang, D. Liu, X. Wang, Y. Song, H. Cao, M. Zeng, Y. Gan, Y. Zhou, Enhanced M1/M2 macrophage ratio promotes orthodontic root resorption, J. Dent. Res. 94 (1) (2015) 129–139.
[69] R.S. Lam, N.M. O'Brien-Simpson, J.C. Lenzo, J.A. Holden, G.C. Brammar, K.A. Walsh, J.E. McNaughtan, D.K. Rowler, N. Van Rooijen, E.C. Reynolds, Macrophage depletion abates Porphyromonas gingivalis-induced alveolar bone resorption in mice, J. Immunol. 193 (5) (2014) 2349–2362.
[70] C. Sima, M. Glogauer, Macrophage subsets and osteoimmunology: tuning of the immunological recognition and effector systems that maintain alveolar bone, Periodontol 63 (1) (2000 2013,) 80–101.
[71] L. Ye, Z. Wen, Y. Li, B. Chen, T. Yu, L. Liu, J. Zhang, Y. Ma, S. Xiao, L. Ding, L. Li, Z. Huang, Interleukin-10 attenuation of collagen-induced arthritis is associated with suppression of interleukin-17 and retinoid-related orphan receptor gammat production in macrophages and repression of classically activated macrophages, Arthritis Res. Ther. 16 (2) (2014) R96.
[72] Y. Yan, X. Lin, X. Dai, G. Wang, L. Zhang, H. Zou, Research progress of regulation of osteoclast formation and function, Zhongguo Xiu Fu Chong Jian Wai Ke Za Zhi 28 (11) (2014) 1435–1440.
[73] A. Sindrilaru, K. Scharffetter-Kochanek, Disclosure of the culprits: macrophages-versatile regulators of wound healing, Adv. Wound Care (New Rochelle) 2 (7) (2013) 357–368.
[74] B.N. Brown, B.D. Ratner, S.B. Goodman, S. Amar, S.F. Badylak, Macrophage polarization: an opportunity for improved outcomes in biomaterials and regenerative medicine, Biomaterials 33 (15) (2012) 3792–3802.
[75] D.C. Palomino, L.C. Marti, Chemokines and immunity, Einstein (Sao Paulo) 13 (3) (2015) 469–473.
[76] J. Dai, A.B. Rabie, VEGF: an essential mediator of both angiogenesis and endochondral ossification, J. Dent. Res. 86 (10) (2007) 937–950.
[77] W. Liu, X. Zhang, Receptor activator of nuclear factor-kappaB ligand (RANKL)/RANK/osteoprotegerin system in bone and other tissues (review), Mol. Med. Rep. 11 (5) (2015) 3212–3218.
[78] S. Fukui, N. Iwamoto, A. Takatani, T. Igawa, T. Shimizu, M. Umeda, A. Nishino, Y. Horai, Y. Hirai, T. Koga, S.Y. Kawashiri, M. Tamai, K. Ichinose, H. Nakamura, T. Origuchi, R. Masuyama, K. Kosai, K. Yanagihara, A. Kawakami, M1 and M2 monocytes in rheumatoid arthritis: a contribution of imbalance of M1/M2 monocytes to osteoclastogenesis, Front Immunol. 8 (2017) 1958.
[79] H. Yuan, J. He, G. Zhang, D. Zhang, X. Kong, F. Chen, Osteoclast stimulatory transmembrane protein induces a phenotypic switch in macrophage polarization suppressing an M1 pro-inflammatory state, Acta Biochim. Biophys. Sin (Shanghai) 49 (10) (2017) 935–944.
[80] K.D. Hankenson, M. Dishowitz, C. Gray, M. Schenker, Angiogenesis in bone regeneration, Injury 42 (6) (2011) 556–561.
[81] A. Page-McCaw, A.J. Ewald, Z. Werb, Matrix metalloproteinases and the regulation of tissue remodelling, Nat. Rev. Mol. Cell Biol. 8 (3) (2007) 221–233.
[82] T.H. Vu, Z. Werb, Matrix metalloproteinases: effectors of development and normal physiology, Genes Dev. 14 (17) (2000) 2123–2133.